Science Translational Medicine
AAAS

www.sciencetranslationalmedicine.org/cgi/content/full/10/432/eaai8524/DC1

# Supplementary Materials for

## The Fas/Fap-1/Cav-1 complex regulates IL-1RA secretion in mesenchymal stem cells to accelerate wound healing

Xiaoxing Kou, Xingtian Xu, Chider Chen, Maria Laura Sanmillan, Tao Cai, Yanheng Zhou, Claudio Giraudo, Anh Le, Songtao Shi*

*Corresponding author. Email: songtaos@upenn.edu

Published 14 March 2018, *Sci. Transl. Med.* **10**, eaai8524 (2018)
DOI: 10.1126/scitranslmed.aai8524

**The PDF file includes:**



**Other Supplementary Material for this manuscript includes the following:**
(available at www.sciencetranslationalmedicine.org/cgi/content/full/10/432/eaai8524/DC1)

Movie S3 (.mov format). TNF-α–activated GMSCs release IL-1RA–positive exosome-like EVs.
Database S1 (.pdf format). Western blotting films corresponding to Figs. 1 to 4.

**Supplementary Materials**

**Materials and methods**

**Electron microscopy (EM)**

For electron microscopy, purified sEVs were left to settle on carbon-coated grids. After staining with 2% uranyl acetate, grids were air-dried and visualized using a transmission electron microscope. Immunogold labeling was performed as previously described (*35*), pelleted sEVs were plated on grids, blocked and stained with anti-IL-1RA antibody (ab124962, 1:50), then incubated in secondary anti-rabbit antibody and labeled with protein A-gold particles (10 nm). Grids were observed using Jeol-1010 Transmission electron microscope.

**Induction of Type 1 Diabetes.** Female C57BL/6J mice aged 8 weeks were injected intraperitoneally with streptozotocin (STZ, Sigma) in dissolved sterile citrate buffer (0.05 mol/L sodium citrate, pH 4.5, 45 mg/kg). STZ or citrate buffer (control) was administered for 5 consecutive days. During the first week of the study, only mice showing consistently elevated blood glucose levels (> 300 mg/dl) were considered diabetic and used for wound experiments (*44*).

**Histology.** To assess wound healing, gingival and cutaneous wound samples were fixed in 4% paraformaldehyde (Sigma-Aldrich) and then decalcified (maxilla samples) with 5% EDTA (pH 7.4), followed by paraffin embedding. Paraffin sections (5 μm) were stained with hematoxylin and eosin (H&E). To perform immunohistochemical staining, the paraffin-embedded sections were blocked with 5% BSA, incubated with the primary antibodies to IL-1RA (Abcam, 1:200) or Fas (Santa Cruz Biotechnology, 1:400) at 4$^{o}$C overnight, and then stained using a VECTASTAIN UNIVERSAL elite ABC kit and ImmPACT VIP Peroxidase Substrate kit (VECTOR) according to the manufacturer's instructions.

**Immunofluorescent staining.** GMSCs were cultured on chamber slides (Nunc) ($1x10^3$/well) and then fixed with 4% paraformaldehyde. The Chamber slides or the previously prepared histological sections were incubated with antibodies at 4$^o$C overnight, then treated with Alexafluoro 568 or Alexafluoro 488 conjugated secondary antibody (1:200, Invitrogen) for 1 hr at room temperature. Finally, slides were mounted with Vectashield mounting medium containing DAPI (Vector Laboratories).

**Enzyme-linked immunosorbent assay (ELISA).** Cell culture medium was collected, and the IL-1RA concentration was analyzed using a mouse ELISA Quantikine Immunoassay kit (R&D Systems MRA00), according to the manufacturer's instructions. For ELISA analysis, culture supernatants (1 ml) from about $0.2x10^6$ MSCs were collected at 48 hrs post culture and the amount of IL-1RA was presented as picograms per $0.2x10^6$ MSCs. The results were averaged within each group. The intra-group differences were calculated between the mean values.

**Cytokine array analysis.** Purified sEV proteins from equal volume of culture supernatant of GMSCs and SMSCs were analyzed using a Mouse Cytokine Array Panel A Array Kit (R&D Systems) according to the manufacturer's instructions. The results were scanned and analyzed using Image J software to calculate blot intensity.

**Real-Time PCR**. Total RNAs were isolated from different GMSCs using TRIzol Reagent (Life Technologies, Invitrogen). RNA samples (1 μg) were reverse-transcribed in a Reverse Transcription system (QIAGEN). Primers used were: *sIl-1ra* forward, 5′-AAATCTGCTGGGGACCCTAC-3′, and reverse 5′- TCCCAGATTCTGAAGGCTTG-3′; *icIl-1ra* forward, 5′-AGACACTGCCTGGGTGCTCCT-3′ and reverse, 5′-GTTTGATATTTGGTCCTTGTAAG-3′; *GAPDH* forward, 5′-GAAGGTGAAGTTCGGAGTC-

3', and reverse 5′- GAAGATGGTGATGGGATTTC-3′. PCR conditions were: 95°C 5 min, (95°C 10 sec, 50°C 45 sec) x 40, and 90°C 10 sec.

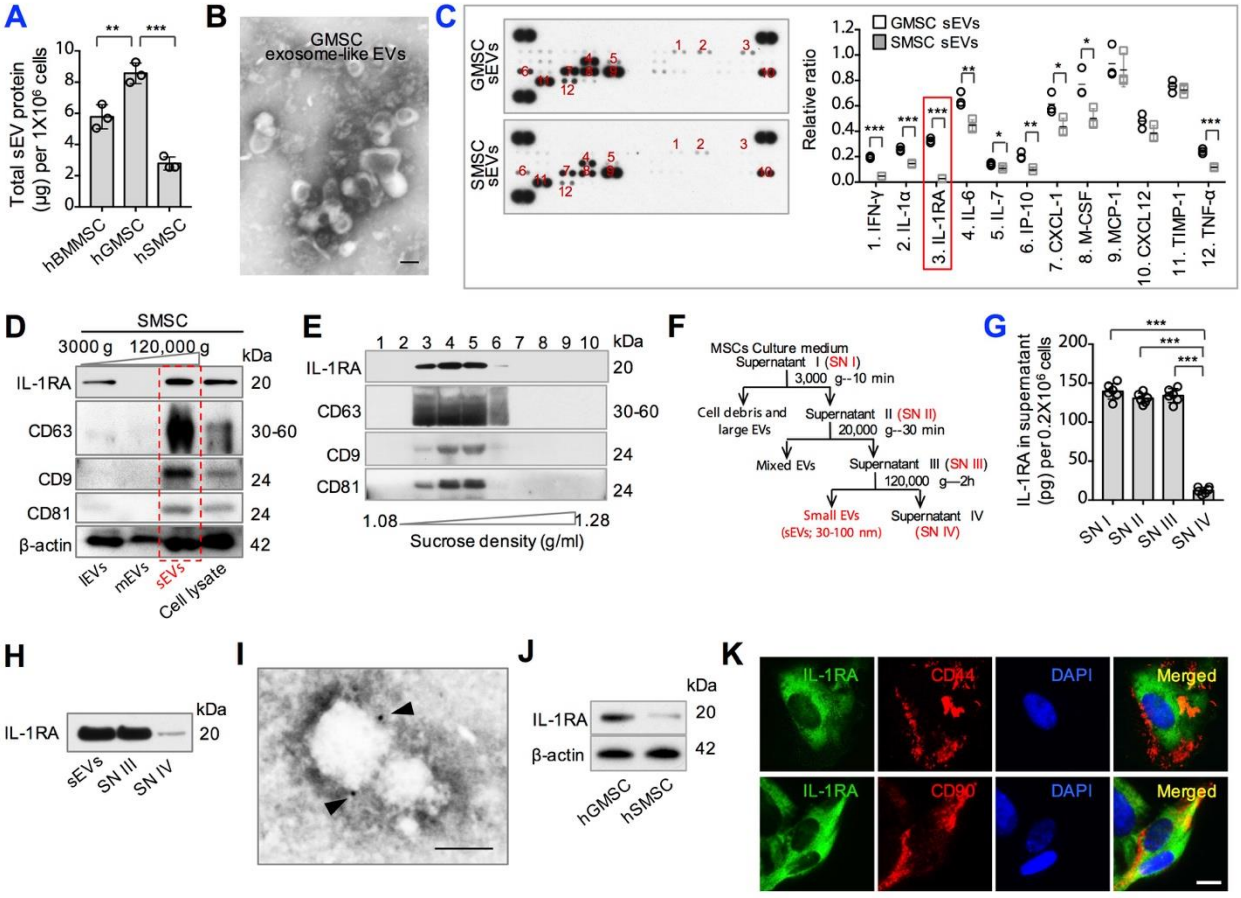


**Fig. S1. GMSCs secrete higher amounts of sEVs and cytokines.** (**A**) Quantification of sEV protein concentration secreted from human BMMSCs, GMSCs and SMSCs (n = 3). (**B**) A representative electron microscopic image of sEVs derived from the culture supernatant of mouse GMSCs. Scale bar, 100 nm. (**C**) Cytokine array analysis of cytokines in sEVs from mouse GMSCs and SMSCs. Equal volumes of sEV protein from GMSCs and SMSCs were loaded for cytokine array (n = 3). (**D**) Western blotting of sEVs, mEVs, lEVs, and cell lysate from mouse SMSCs. The total proteins as defined in Fig. 1D were subjected to Western blot analysis. (**E**) Crude EVs from mouse GMSCs were isolated by step sucrose gradient (1.08-1.28 g/ml, that is, 0.8 to 2 M), and 10 fractions were collected for Western blotting analysis. (**F**) Differential centrifugation procedure for the isolation of sEVs from mouse MSC culture supernatants. (**G, H**)

ELISA and Western blotting analysis of the supernatants and sEVs after different steps of centrifugation as indicated in (F) (n = 3). (**I**) Electron microscopic for immunogold labelling of purified sEVs with anti-IL-1RA antibodies. Arrowhead indicated IL-1RA positive sEVs. Scale bar, 100 nm. (**J**) Western blotting of human GMSCs and human SMSCs, cytoplasmic lysates. (**K**) Immunocytofluorescence staining for co-expression of IL-1RA (green) with CD44 or CD90 (red) in WT GMSCs. Cell nucleus were counterstained with DAPI (blue). Scale bar, 20 μm. All results are representative of data generated in at least three independent experiments. **P< 0.01; ***P< 0.001. Error bars are mean ± SD. Data were analyzed using one-way ANOVA with the Bonferroni correction (A, G), or independent unpaired two-tailed Student's t-tests (C).

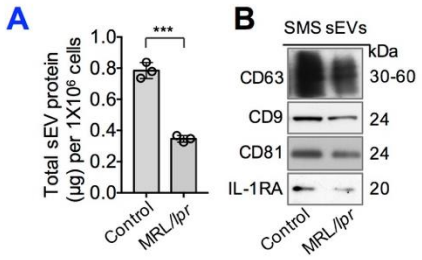


**Fig. S2. Fas controls IL-1RA–sEV secretion in murine SMSCs. (A)** Quantitation of sEV protein secreted into the culture supernatant from Fas-deficient-MRL/*lpr* and control (WT) SMSCs (n = 3). ***P< 0.001. Error bars are mean ± SD. Data were analyzed using independent unpaired two-tailed Student's t-tests. **(B)** Western blotting of equal number of Fas-deficient-MRL/*lpr* SMSCs-derived sEVs for CD63, CD9, CD81, and IL-1RA compared to WT control SMSC-derived sEVs. All results are representative of data generated in at least three independent experiments.

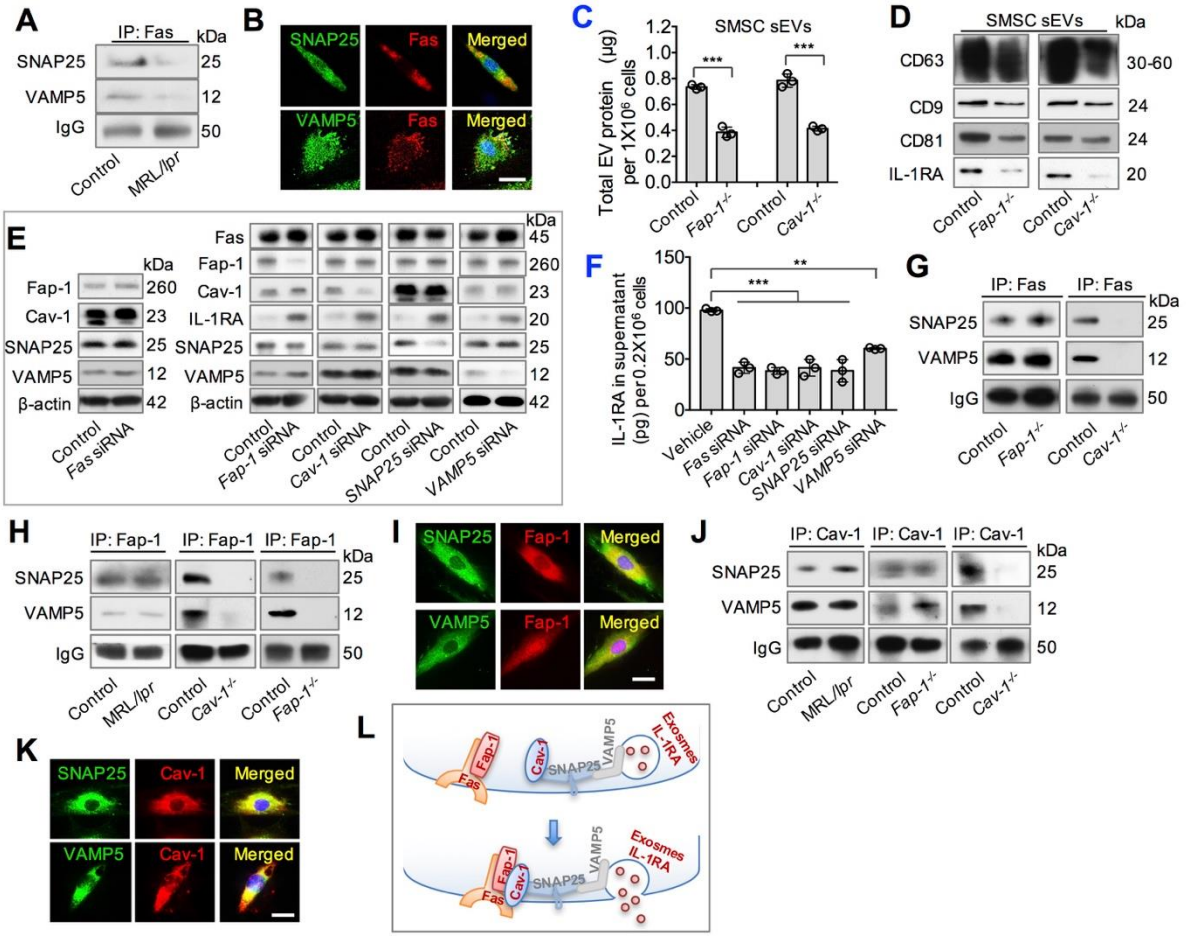


**Fig. S3. Fas/Fap-1 binds with Cav-1 to control SNAP25/VAMP5-mediated IL-1RA release in murine MSCs.** (**A**) Immunoprecipitation analysis of Fas, SNAP25, and VAMP5 in WT and MRL/*lpr* GMSC whole cell lysates. IP, immunoprecipitation. (**B**) Immunocytofluorescence staining for co-localization of Fas with SNAP25 and Fas with VAMP5 in WT GMSCs. (**C**) Quantification of secreted sEV proteins in WT control, *Fap-1* and *Cav-1* knockout SMSCs (n = 3). (**D**) Western blotting of sEV from *Fap-1* and *Cav-1* knockout SMSCs compared to WT control SMSCs. sEV-associated proteins from the culture supernatant of equal number of cells from control and knockout SMSCs were loaded for Western blot analysis. (**E**) Western blotting of *Fas*, *Fap-1*, *Cav-1*, *SNAP25*, and *VAMP5* siRNA-treated GMSCs compared to WT. (**F**) ELISA analysis secreted IL-1RA in supernatant of *Fas*, *Fap-1*, *Cav-1*, *SNAP25* and *VAMP5* siRNA-treated GMSCs compared to the vehicle control group (n = 3). (**G**) Immunoprecipitation analysis of Fas, SNAP25, and VAMP5 in *Fap-1* and *Cav-1* knockout GMSCs compared to WT control. (**H**) Immunoprecipitation analysis of Fap-1, SNAP25, and VAMP5 in MRL/*lpr*, *Fap-1* knockout or *Cav-1* knockout GMSCs compared to WT control. (**I**) Immunocytofluorescence double staining for co-localization of Fap-1, SNAP25 and VAMP5 in WT GMSCs. (**J**) Immunoprecipitation analysis of Cav-1, SNAP25, and VAMP5 in MRL/*lpr*, *Fap-1* knockout or *Cav-1* knockout GMSCs compared to WT control. (**K**) Immunocytofluorescence double staining for co-localization of Cav-1, SNAP25, and VAMP5 in WT GMSCs. For immunoprecipitation, whole cell lysates from indicated GMSCs were immunoprecipitated with corresponding antibodies, and the immunocomplexes were subjected to Western blot analysis with antibodies

against SNAP25 and VAMP5. IP, immunoprecipitation. (**L**) Schematic diagram of the Fas/Fap-1/Cav-1 machinery controlling IL-1RA secretion. The Fas/Fap-1 complex binds with Cav-1, and then binds with the SNAP25/VAMP5 complex to control the secretion of exosome/IL-1RA. Cytoplasmic distribution of Cav-1 was affected by Fas and Fap-1. All results are representative of data generated from three independent experiments. **P< 0.01; ***P< 0.001. Error bars are mean ± SD. Data were analyzed using independent unpaired two-tailed Student's t-tests. Scale bars, 20 μm.

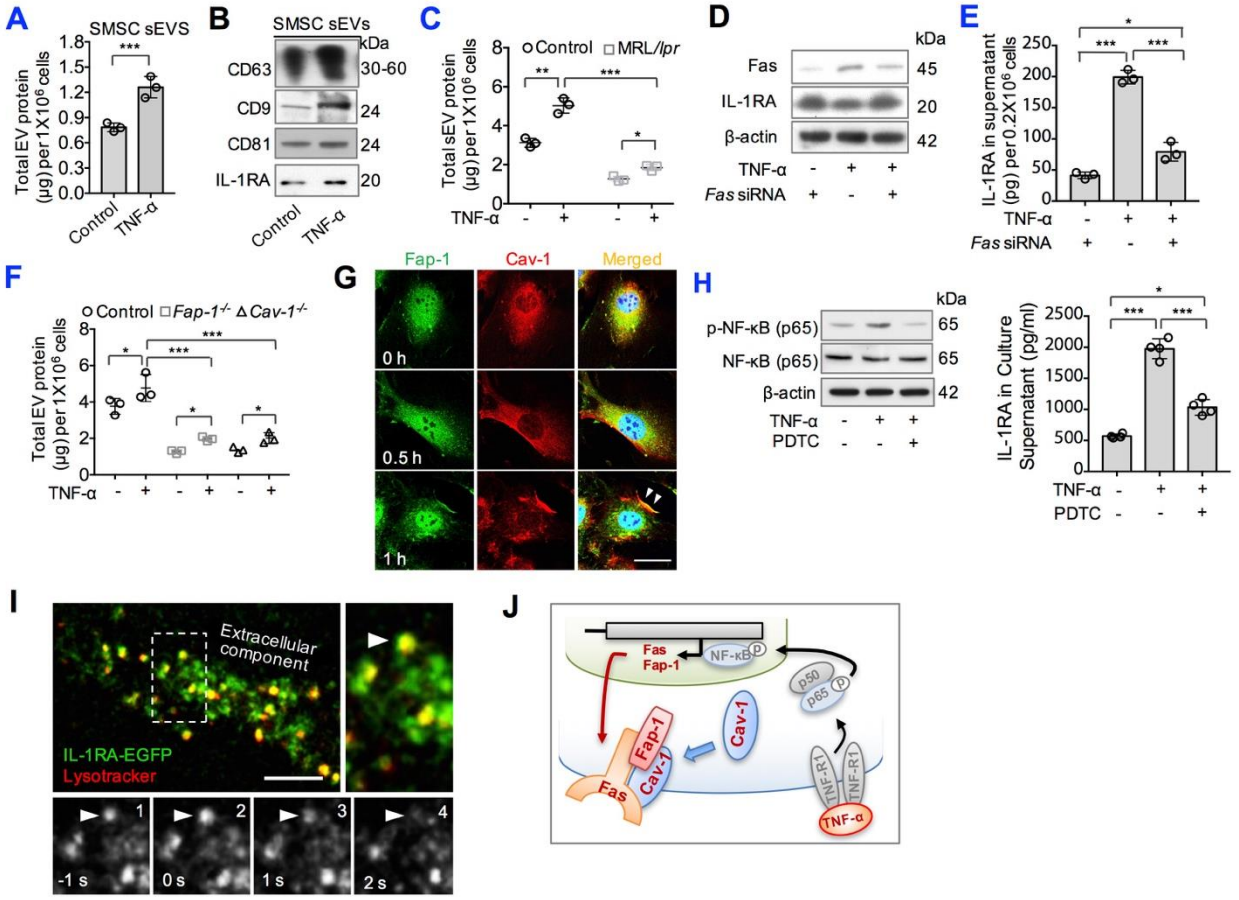


**Fig. S4. TNF-α promotes sEV and IL-1RA release in murine MSCs.** (**A**) Quantitation of sEV protein secreted into the culture supernatant of control or TNF-α (20 ng/ml)-treated SMSCs (n = 3). (**B**) Western blotting of CD63, CD9, CD81, and IL-1RA expression in WT control SMSCs with or without TNF-α (20 ng/ml) treatment. sEV proteins from the culture supernatant of equal number of cells were loaded for the Western blot analysis. (**C**) Quantitation of sEV proteins secreted into the culture supernatant of control and MRL/lpr GMSCs with or without TNF-α (20 ng/ml) treatment (n = 3). (**D**) Western blotting of IL-1RA expression in WT GMSC and *Fas* siRNA-treated GMSC with or without TNF-α (20 ng/ml) treatment. (**E**) ELISA analysis of IL-1RA in the culture supernatant of WT GMSC and *Fas* siRNA-treated GMSC with or without TNF-α (20 ng/ml) treatment (n = 3). (**F**) Quantitation of sEV protein secreted into the culture supernatant from WT control, Fap-1 and Cav-1 knockout GMSCs treated with or without TNF-α (20 ng/ml) (n = 3). (**G**) Immunocytofluorescence staining of GMSCs at various time points after TNF-α (20 ng/ml) treatment. Scale bar, 20 μm. (**H**) Western blotting of phosphorylated-NF-κB p65 expression in WT GMSC treated with or without TNF-α (20 ng/ml) and NF-κB inhibitor PDTC as indicated in the left panel. ELISA analysis of IL-1RA in the culture supernatant of WT GMSC treated with or without TNF-α (20 ng/ml) and NF-κB inhibitor PDTC as indicated in the right panel (n = 4). (**I**) TIRF microscopy images of IL-1RA-EGFP (green) transfected into WT GMSC and stained with lysotracker fluorescence (red). The upper right panel is a higher magnification of the boxed region in the left image to show co-localization (yellow); the lower

panel shows sequential images (1 to 4). Arrowheads indicate the IL-1RA-positive vesicle fusion event. Scale bar, 10 μm. (J) Schematic diagram of TNF-α regulated EV and IL-1RA release. All results are representative of data generated from three independent experiments. *P<0.05; **P< 0.01; ***P< 0.001. Error bars are mean ± SD. Data were analyzed using independent unpaired two-tailed Student's t-tests (A, C and F), or one-way ANOVA with the Bonferroni correction (E, H).

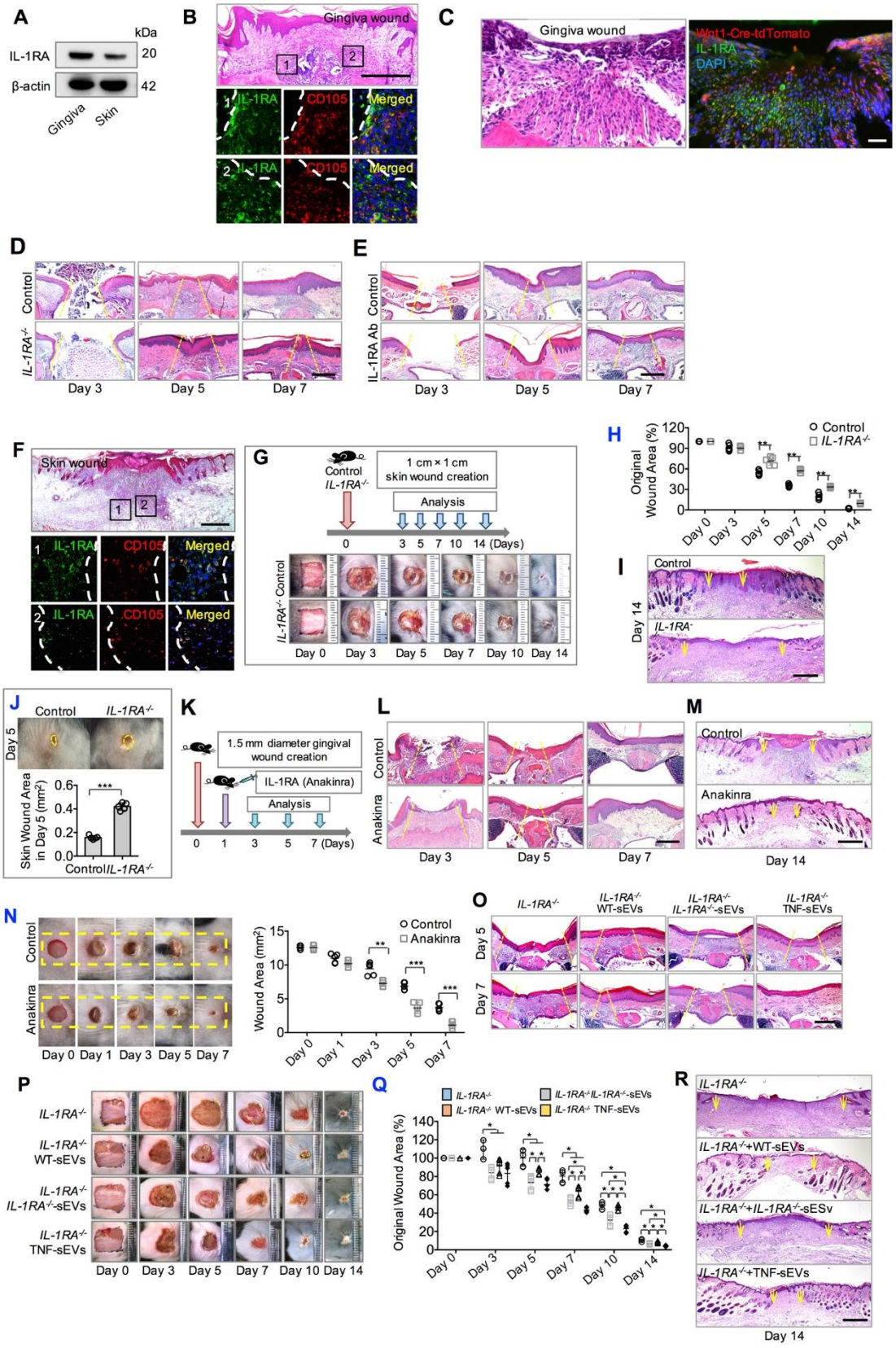
A
kDa
IL-1RA
20
β-actin
42
Gingiva
Skin
B
Gingiva wound
1
2
IL-1RA
CD105
Merged
C
Gingiva wound
Wnt1-Cre-tdTomato
IL-1RA
DAPI
D
Control
IL-1RA-/-
Day 3
Day 5
Day 7
E
Control
IL-1RA Ab
Day 3
Day 5
Day 7
F
Skin wound
G
Control
IL-1RA-/-
1 cm × 1 cm
skin wound creation
Analysis
0 3 5 7 10 14 (Days)
Day 0 Day 3 Day 5 Day 7 Day 10 Day 14
H
Original Wound Area (%)
Control
IL-1RA-/-
Day 0 Day 3 Day 5 Day 7 Day 10 Day 14
I
Day 14
Control
IL-1RA-
J
Control
IL-1RA-/-
Day 5
Skin Wound Area in Day 5 (mm2)
Control IL-1RA-/-
K
1.5 mm diameter gingival
wound creation
IL-1RA (Anakinra)
Analysis
0 1 3 5 7 (Days)
L
Control
Anakinra
Day 3
Day 5
Day 7
M
Control
Anakinra
Day 14
N
Control
Anakinra
Day 0 Day 1 Day 3 Day 5 Day 7
Wound Area (mm2)
Control
Anakinra
O
IL-1RA-/-
IL-1RA-/- WT-sEVs
IL-1RA-/- IL-1RA-/--sEVs
IL-1RA-/- TNF-sEVs
Day 5
Day 7
P
IL-1RA-/-
IL-1RA-/- WT-sEVs
IL-1RA-/- IL-1RA-/--sEVs
IL-1RA-/- TNF-sEVs
Day 0 Day 3 Day 5 Day 7 Day 10 Day 14
Q
IL-1RA-/-
IL-1RA-/- WT-sEVs
IL-1RA-/- IL-1RA-/--sEVs
IL-1RA-/- TNF-sEVs
Original Wound Area (%)
Day 0 Day 3 Day 5 Day 7 Day 10 Day 14
R
IL-1RA-/-
IL-1RA-/-+WT-sEVs
IL-1RA-/-+IL-1RA-/--sESv
IL-1RA-/-+TNF-sEVs
Day 14

**Fig. S5. Histomorphology of IL-1RA in wound healing in mice.** (**A**) Western blotting of IL-1RA in gingival and skin wound tissue. (**B**) Immunohistofluorescence double staining for co-localization of IL-1RA and CD105 in gingival wound areas. Lower panels are higher magnification views of immunostaining images from the boxed region in the upper H&E image, indicating co-expression of IL-1RA (green) and CD105 (red) near the margin of the wound area. Dashed lines indicate the margin of the wound healing area. (**C**) Immunohistofluorescence staining of IL-1RA in gingiva wounds of Wnt1-Cre-tdTomato mice. (**D**) Representative H&E image from gingival wounds in WT control and *IL-1RA*$^{-/-}$ mice in Fig. 5B. (**E**) Representative H&E image from WT control and IL-1RA antibody-treated gingival wounds in Fig. 5C. (**F**) Immunohistofluorescence double for co-localization of IL-1RA and CD105 in cutaneous wound tissue. Lower panels are higher magnification views of immunostaining images from the boxed region in the upper H&E image, indicating co-expression of IL-1RA (green) and CD105 (red) near the margin of the wound area. Dashed lines indicate the margin of the wound healing area. (**G**) Scheme depicting the cutaneous wound procedure in *IL-1RA*$^{-/-}$ mice. Full-thickness excision cutaneous wounds (1 cm × 1 cm) were created in the mid-backs of WT control and *IL-1RA*$^{-/-}$ mice (upper panel). Representative photos of full-thickness cutaneous wounds in WT control and *IL-1RA*$^{-/-}$ mice after wound creation are shown in the lower panel. (**H**) Percentage of the wound closure on day 3 to day 14 in reference to the day 0 wounds from the groups described in (**G**) (n = 5). (**I**) Representative H&E image from a cutaneous wound in fig. S5G. **(J)** Photos and quantification of cutaneous wound area in *IL-1RA*$^{-/-}$ mice compared to control WT mice 5 days after wounding (n = 5). (**K**) Scheme illustrating the gingival wound procedure and treatment with IL-RA drug Anakinra. WT mice were submucosally injected with either placebo (0.9% saline) or IL-1RA drug Anakinra (100 μg per mouse) one day after wound creation. Representative H&E image from a gingival wound in Fig. 5D **(L)** and cutaneous wound in Fig. 5F (**M**). (**N**) Photo images and quantification of cutaneous wound area in WT mice injected with either placebo (0.9% saline) or IL-1RA drug (Anakinra, 500 μg per mice) one day after wound creation (n = 5). (**O**) Representative H&E image from a gingiva wound in Fig. 5M. (**P**) Representative photos of full-thickness cutaneous wounds in IL-1RA knockout mice after treatment with WT control SMSC-derived, IL-1RA knockout SMSC-derived, or TNF-α-activated SMSC-derived sEVs compared to no treatment. (**Q**) Percentage of the wound closure from the groups described in (P) (n = 5). (**R**) Representative H&E image from the cutaneous wound in fig. S5P. All results are representative of data generated from three independent experiments. Scale bars, 200 μm (B-E, L, O), or 500 μm (F, I, M, R). *P<0.05; **P< 0.01; ***P< 0.001. Error bars are mean ± SD. Data were analyzed using independent unpaired two-tailed Student's t-tests (H, J, N), or one-way ANOVA with the Bonferroni correction (Q).

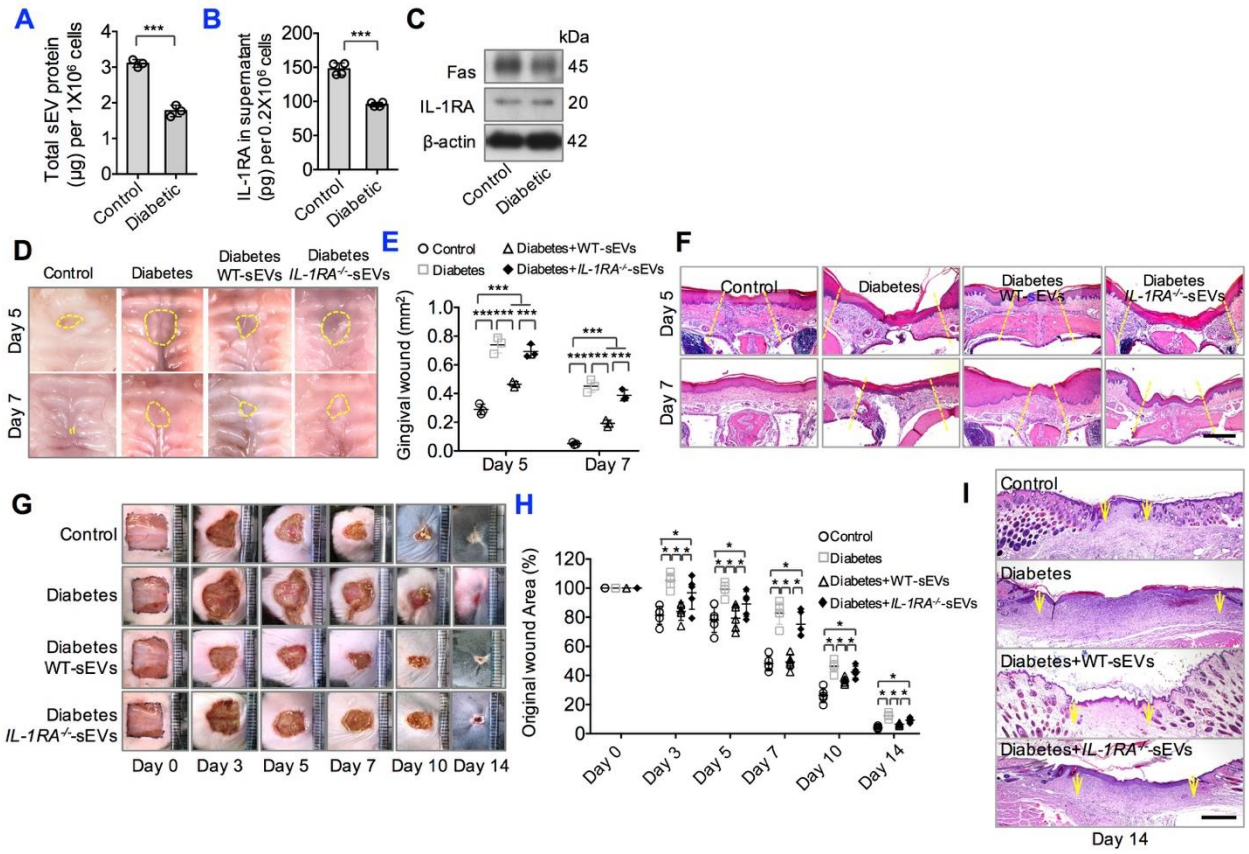


**Fig. S6. sEVs containing IL-1RA ameliorate delayed wound healing in diabetic mice.** (**A**) Quantification of secreted sEV proteins in GMSCs from control and diabetic mice (n = 3). (**B**) ELISA analysis of IL-1RA secretion in the culture supernatant of GMSCs from control and diabetic mice (n = 4). (**C**) Western blotting of Fas and IL-1RA expression in GMSCs from control and diabetic mice. (**D**) Representative macroscopic images of gingival wound area in control mice and diabetic mice treated with placebo (0.9% saline) or WT GMSC-derived, or IL-1RA knockout GMSC derived sEVs. (**E**) Quantification of the gingival wound area in each group, as defined in (D) (n = 3). (**F**) Representative H&E image from a gingiva wound in fig. S6D. (**G**) Representative photos of full-thickness cutaneous wounds in control mice and diabetic mice treated with placebo (0.9% saline) or WT GMSC-derived, or IL-1RA knockout GMSC derived sEVs. (**H**) Percentage of wound closure from the groups described in (G) (n = 5). (**I**) Representative H&E image from the cutaneous wound in fig. S6G. All results are representative of data generated from three independent experiments. **P*<0.05. Error bars are mean ± SD. Scale bars, 200 μm (**F**), or 500 μm (**I**). *P<0.05; **P< 0.01; ***P< 0.001. Error bars are mean ± SD. Data were analyzed using independent unpaired two-tailed Student's t-tests (A, B), or one-way ANOVA with the Bonferroni correction (E, H).

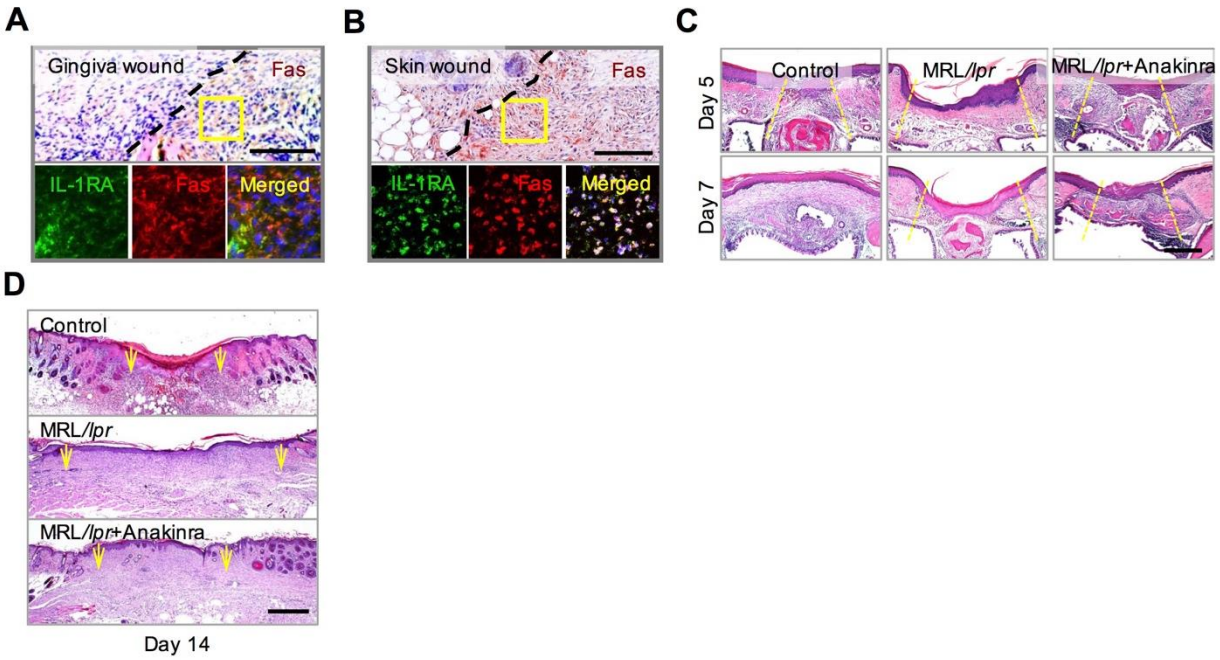


**Fig. S7. Histomorphology of Fas in wound healing in mice.** (**A, B**) Immunohistofluorescence double staining for co-localization of IL-1RA and Fas in gingival and cutaneous wound tissue after wounding. Dash lines indicated the margin of wound healing area. Lower panels are a higher magnification of immunostaining images from the boxed region in the upper IHC images, indicating a strong co-expression of IL-1RA (green) and Fas (red) near the margin of wound area. (**C, D**) Representative H&E image from gingival wound for Fig. 6B and cutaneous wound for Fig. 6, C and D. All results are representative of data generated from three independent experiments. Scale bars, 200 μm.

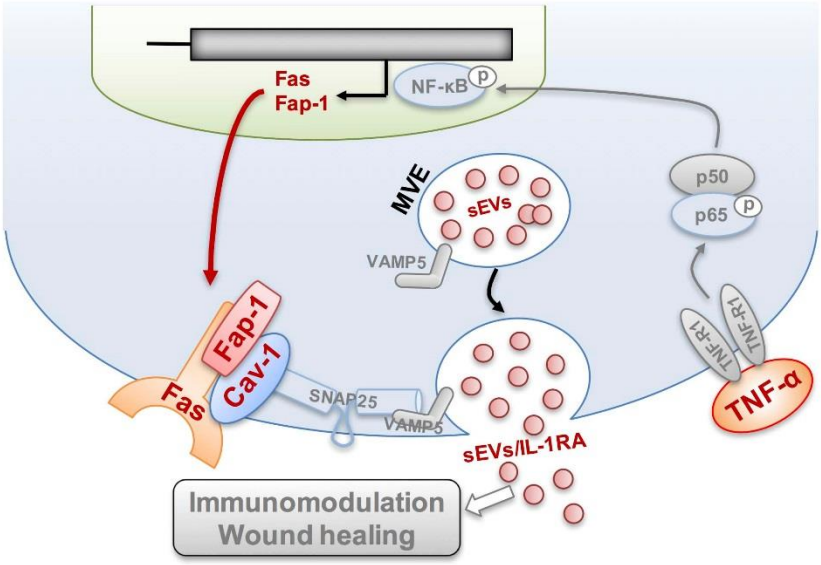


**Fig. S8. Schematic drawing of Fas/Fap-1/Cav-1–controlled IL-1RA–sEV secretion in MSCs.** MVE: Multivesicular endosomes; sEVs: small extracellular vesicles; IL-1RA: Interleukin 1 receptor antagonist; Fap-1: Fas associate phosphatase 1; Cav-1: Caveolin-1.

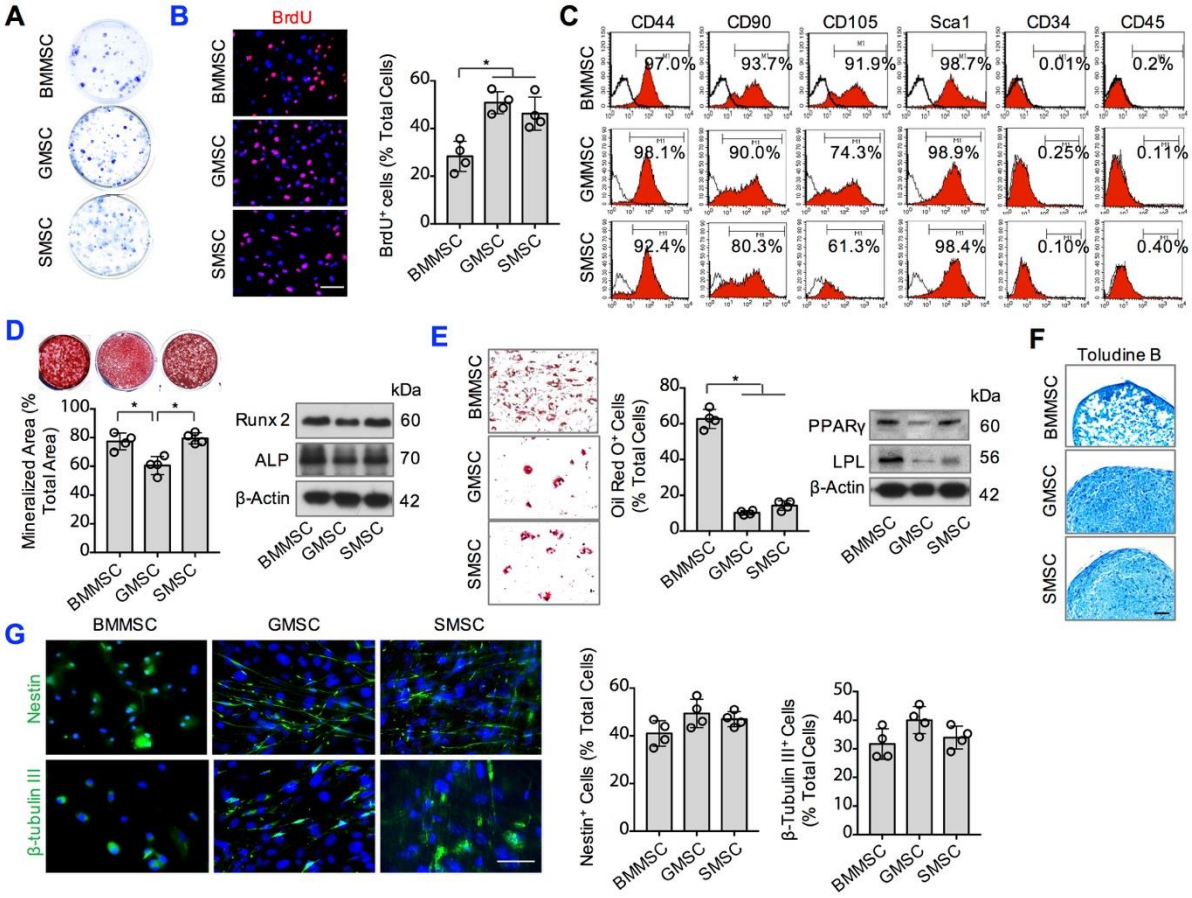


**Fig. S9. Characterization of BMMSCs, GMSCs, and SMSCs. (A, B)** Analysis of mouse BMMSCs, GMSCs, and SMSCs CFU-F formation and proliferation. **(C)** Flow cytometric analysis of MSCs for mesenchymal stem cell surface markers CD44, CD90, CD105, and Sca-1, and the hematological markers CD34 and CD45. **(D)** Osteogenic, **(E)** adipogenic, **(F)** chondrogenic, and **(G)** neurogenic differentiation assays using the MSCs.

**Supplementary Movie Legends**

**Movie S1. GMSCs secrete IL-1RA–positive exosome-like EVs.** WT GMSCs were co-transfected with plasmids expressing IL-1RA-EGFP fusion protein and CD63-mCherry fluorescent protein. The video was acquired by TIRF microscopy, showing that IL-1RA-EGFP/CD63-mCherry double-positive exosome-like EVs fused with the plasma membrane in living GMSCs.

**Movie S2. Exocytotic fusions of IL-1RA–positive vesicles in living GMSCs.** WT GMSCs were transfected with plasmids expressing IL-1RA-enhanced green fluorescent protein (IL-1RA-EGFP) and the vesicular organelles were stained with lysotracker fluorescence. The video was acquired by TIRF microscopy, showing IL-1RA-EGFP-positive vesicles fusing with the plasma membrane in living GMSCs after treatment with TNF-α (20 ng/ml) for 0.5 hour. Arrows indicate intensive fusion events occurring on the membranes of GMSCs.

**Movie S3. TNF-α–activated GMSCs release IL-1RA–positive exosome-like EVs.** WT GMSCs were co-transfected with plasmids expressing IL-1RA-EGFP fusion protein and CD63-mCherry fluorescent protein. The video was acquired by TIRF microscopy, showing that IL-1RA-EGFP/CD63-mCherry double-positive exosome-like EVs fused with the plasma membrane in living GMSCs after treatment with TNF-α (20 ng/ml) for 0.5 hour. Arrows indicate intensive fusion events occurring on the membranes of GMSCs.